UC Davis
UC Davis Previously Published Works

Title

Temporal Variability of Emissions Revealed by Continuous, Long-Term Monitoring of an Underground Natural Gas Storage Facility

Permalink

https://escholarship.org/uc/item/3tc8r8n4

Journal

Environmental Science and Technology, 54(22)

ISSN

0013-936X

Authors

Alden, Caroline B
Wright, Robbie J
Coburn, Sean C
et al.

Publication Date

2020-11-17

DOI

10.1021/acs.est.0c03175

Peer reviewed

Temporal Variability of Emissions Revealed by Continuous, Long-Term Monitoring of an Underground Natural Gas Storage Facility

Caroline B. Alden,* Robbie J. Wright, Sean C. Coburn, Dani Caputi, Griffith Wendland, Alex Rybchuk, Stephen Conley, Ian Faloona, and Gregory B. Rieker

Cite This: https://dx.doi.org/10.1021/acs.est.0c03175

Read Online

ACCESS | Metrics & More | Article Recommendations | Supporting Information

ABSTRACT: Temporal variability contributes to uncertainty in inventories of methane emissions from the natural gas supply chain. Extrapolation of instantaneous, "snapshot-in-time" measurements, for example, can miss temporal intermittency and confound bottom-up/top-down comparisons. Importantly, no continuous long-term datasets record emission variability from underground natural gas storage facilities despite substantial contributions to sector-wide emissions. We present 11 months of continuous observations on a section of a storage site using dual-frequency comb spectroscopy (DCS observing system) and aircraft measurements. We find high emission variability and a skewed distribution in which the 10% highest 3 h emission periods observed by the continuous DCS observing system comprise 41% of the total observed 3-hourly emissions. Monthly emission rates differ by >12×, and 3-hourly rates vary by 17× in 24 h. We find links to the operating phase of the facility—emission rates, including as a percentage of the total gas flow rate, are significantly higher during periods of injection compared to those of withdrawal. We find that if a high frequency of aircraft flights can occur, then the ground- and aircraft-based approaches show excellent agreement in emission distributions. A better understanding of emission variability at underground natural gas storage sites will improve inventories and models of methane emissions and clarify pathways toward mitigation.
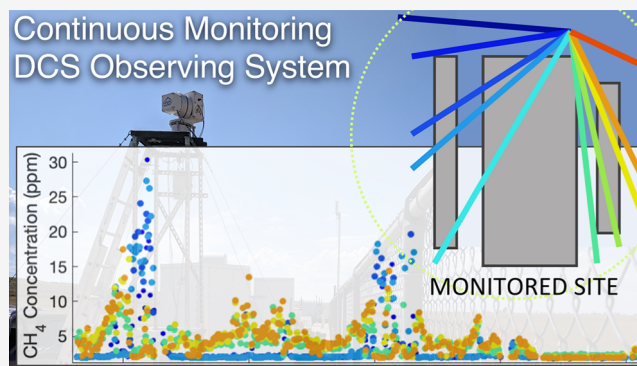
1. INTRODUCTION

Natural gas is an important energy source in the United States, comprising 28.6% of the total U.S. energy use in 2017.[1] Recently, increased scientific, regulatory, societal, and industry attention has focused on emissions of methane along the natural gas supply chain, which threaten to undermine the benefits of natural gas as a relatively lower carbon-to-energy fuel source (compared with coal)[2,3] and which can negatively impact regional air quality.[4,5] The reduction of methane emissions from oil and gas represents a relatively achievable short-term mitigation goal in comparison with longer-term control of emissions from other industries.[6] Independent assessments of emissions have revealed mismatches between bottom-up (e.g., inventory-based) and top-down (e.g., atmospheric measurement-based) estimates across the natural gas sector, from production wells to urban distribution systems.[7,8] Several new studies suggest that temporal variability in emissions as well as a fat-tailed distribution of high-emitting fugitive events can contribute to disagreements in emission estimates and that accounting for these sources of spatial and temporal variability can help to reconcile flux estimates.[9–13]

Better understanding of temporal variability in methane emissions from oil and gas infrastructure has been identified as

an important area for improvement in the Environmental Protection Agency (EPA) Greenhouse Gas Inventory (GHGI).[14] Yet, high levels of uncertainty remain in our understanding of temporal characteristics of emissions. Continuous monitoring, in particular, has been identified as a critical tool for a better understanding of the temporal profile of emissions at natural gas facilities.[15] New state-level regulations in Colorado go so far as to mandate continuous monitoring of oil and gas facilities.[16]

While variability in emissions from the production and processing sector of the natural gas supply chain has been increasingly confirmed,[17] emissions from underground natural gas storage facilities have not been studied as extensively. Though there are relatively few storage facilities (~400 in the United States[18]), the transmission and storage sector is estimated to contribute a substantial proportion of value-
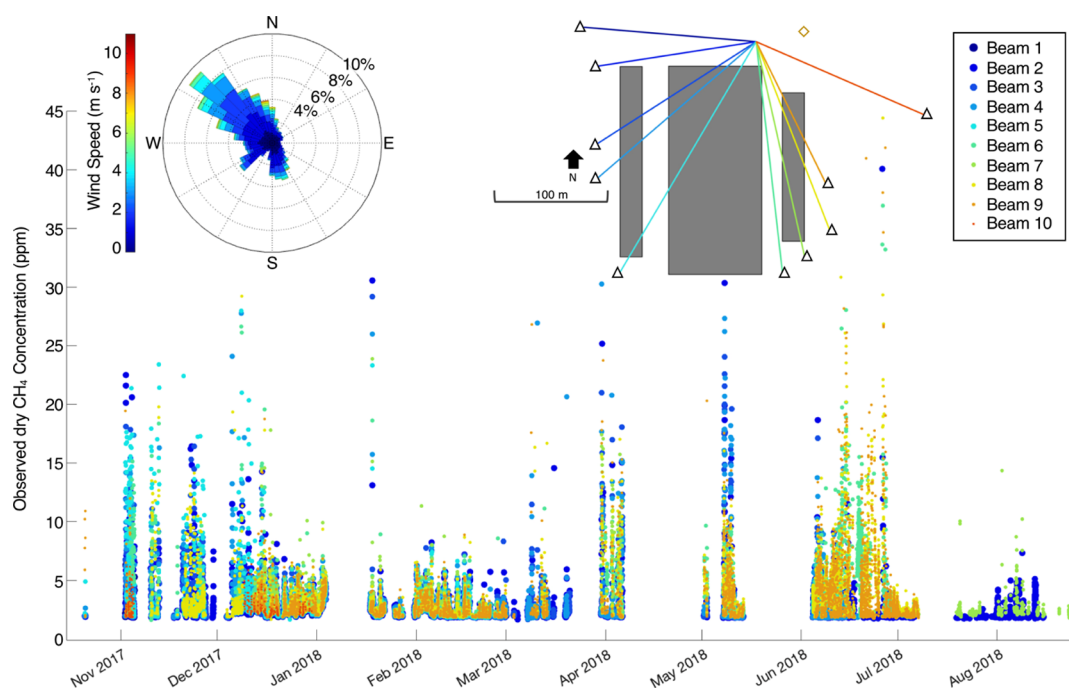
Figure 1. Time series of atmospheric observations of CH_4 concentrations along the DCS laser beam paths. The beam path and site layout are shown in a map-view inset at the upper right, including three gray areas with well heads (left box), gas conditioning equipment (middle box), and well heads (right box). Black triangles show the locations of retroreflectors and the yellow diamond shows the location of an anemometer. The inset in the upper left shows a wind rose of meteorological conditions during the observation period. The legend shows the laser beam colors and marker sizes as they relate to the site layout and concentration data.

chain emissions (20%[1]) and has garnered attention because of the recent high-profile Aliso Canyon extreme emission event.[19,20] Storage of natural gas in underground reservoirs has been practiced in the United States for over 100 years to supplement pipeline delivery during periods of variable supply and demand.[21] Storage reservoirs are primarily porous rock reservoirs (e.g., depleted oil and gas fields or aquifers) and salt caverns[18] into which gas is injected or from which it is withdrawn to level supply/demand, such as during cold snaps.[21] Gas storage is increasingly also used to meet higher-frequency changes in electricity generation, supplementing other energy sources with more variable supply (e.g., renewables).[22]

Detailed examination of emissions from specific equipment at underground storage facilities has been limited in time and has focused primarily on compressor stations.[23,24] Repeated flyover measurements of emissions from underground natural gas storage sites do, however, suggest the possibility of high emission variability.[25] For example, one recent study demonstrated emission rates that differed by up to 6× on contiguous days at the same site.[25,26]

In this study, we perform the first continuous monitoring of emissions from a portion of an underground natural gas storage facility using local atmospheric trace gas concentration measurements and inversions with a ground-based dual-frequency comb spectrometry (DCS) observing system (hereafter DCS observing system). We also perform concurrent, repeat aircraft mass balance flights for cross-validation of methods. Finally, we compare the resulting time series of estimated emissions with operations data collected by the storage site managers.

2. EXPERIMENTAL METHODS

To assess emissions and variability at an underground natural gas storage site, we deployed two sensor systems for a period of 11 months, from October 2017 through August 2018. The first is a ground-based sensor system that continuously and autonomously monitors emissions (DCS observing system, Section 2.2) and the second is an aircraft-based trace gas sensor flown for mass balance "snapshot-in-time" emission estimation (Section 2.3). The ground-based sensor is a long-range, open-path DCS. The DCS data are coupled with atmospheric inversions to determine emission source locations and rates.[27−29] The aircraft-based sampling approach relies on methods developed and tested at similar sites.[19,25,30] Both are described in greater detail below.

2.1. Underground Natural Gas Storage Site Layout. The study site is an underground natural gas storage facility located in the U.S. Energy Information Administration (EIA) Pacific Region. The site is in the top quartile of all storage sites in the United States in terms of both base gas storage (the "permanent" inventory used to maintain the storage reservoir pressure) and total field capacity (the maximum reservoir storage capacity).[18] Continuous DCS observing system measurements and repeat aircraft mass balance flights focused on an isolated section of infrastructure on the site, which allowed for a clear constraint of signals against background emissions from neighboring sites (Figure 1). The portion of the storage site studied houses well heads and gas conditioning equipment (Figure 1 and Supporting Information Section 1 for more details regarding on-site equipment). The nearest compressors are >500 m away in a different area of the site. The study area contains just over 40% of the total well heads on the whole site and just over 20% of the filter separators, and the spatial extent of the study area covers roughly 10% of the

full extent of the underground formation. Equipment heights in the study area range from roughly ground-height to roughly 13 m above the ground.

2.2. Ground-Based DCS Observing System Measurements and Data Reduction. The DCS observing system collects continuous, high-frequency atmospheric concentration measurements and atmospheric inversions yield emission rates and locations with a 3 h resolution.

A single DCS laser housed in a small trailer was placed on the north edge of a section of the above-ground infrastructure associated with the storage site (Section 2.1, Figure 1). A laser light pitch and catch system was positioned on a small retractable tower. A set of 10 retroreflective mirrors was fixed to the existing infrastructure on the site, enabling 10 integrated open paths or "beams" that extended between the laser head and each retroreflector (Figure 1). After 11 months, minor degradation of return power was observed from dust accumulation on the retroreflectors, with no impact on measurement precision or reliability. Infrequent, heavy rain occluded the line-of-sight to the retroreflectors, and morning dew occasionally and temporarily blocked the telescope window until evaporation took place. Observations were taken along one beam path at a time in sequence, and measurements were averaged for 120−180 s. Beam heights varied between 1 and 3 m above the ground level. An RM Young 81000 3D sonic anemometer was stationed at a 10 m standoff distance from the DCS to collect meteorological observations for use in the inversion (Figure 1).

DCS is a spectroscopic method that measures extremely high-resolution (0.0018 nm or 200 MHz) absorption spectra, which can be used to determine accurate and precise information about concentrations of molecular trace gases along the beam path.[31] The laser light is eye-safe and invisible. The precision of the concentration measurements during this campaign was on the order of 5−30 ppb. Critically, instrument calibration is not needed for DCS in this application because we are measuring differential enhancements among laser beams (overcoming small absolute biases of the spectroscopic model used for concentration retrieval) and because the DCS wavelength, phase noise, and return power are all continuously monitored and controlled to eliminate drift or distortion of the measured spectrum.[32] The atmospheric data (which consist of both methane and water vapor concentrations) are processed to provide dry-air path-averaged mole fractions (concentrations) of methane using spectroscopic fits to the HITRAN 2008 database. The broad wavelength range afforded by DCS (178.8−185.5 THz or 1625−1675 nm), combined with the extremely high resolution (200 MHz), allows for the simultaneous fitting of approximately 3240 individual H_2O (133), CH_4 (625), and CO_2 (2482) absorption features. This allows for a precise intercomparison of observations made on different instruments and across different time periods.[32,33] The concentration information generated in this way is used in an atmospheric inversion algorithm, which solves for the locations and rates of emissions in the monitored area. Background or baseline concentrations are removed, yielding CH_4 enhancements that are then fitted using a Gaussian plume model to parameterize atmospheric transport.[27] Potential emission sources are parsed from the areas in the gray boxes in Figure 1 into groupings of equipment, with heights assigned accordingly. The use of this system for emission quantification in blinded validation tests and at oil and gas sites has been described in several recent publications.[29,34]

We solve for emissions with 3-hourly resolution to balance data density (maximizing the number of measurements available for inversion, given the high number of beams sampled to cover a large facility) with a temporal resolution that allows for analysis of subdaily emission variability; a higher or a lower temporal resolution is possible via the balance of these two trade-offs.

Data analysis for the DCS observing system involves several steps. First, atmospheric inversions with a range of parameter choices are performed to estimate the error bounds of the emission calculation. Specifically, an ensemble of five atmospheric inversions is used, following recently published work using the DCS observing system[27−29,34] (full details in Supporting Information Section 3). Second, an analysis of site coverage is performed to guide the interpretation of the results. Changing wind conditions can result in a greater or lesser sensitivity of line-integrated measurements to emission sources at various locations on the storage site because of the geometry of the site layout. That is, the "fetch" of the area surveyed with each measurement changes based on the meteorological conditions of each measurement. Indeed, this phenomenon is a factor common to all atmospheric concentration-based observing systems and one that is particularly important for point sensor arrays that cannot offer integrated path-averaged coverage. For example, when the prevailing wind direction is from the north, plumes from some areas are less likely to cross any laser beam measurement paths ("beam") such that not all areas in the gray boxes in Figure 1 would be covered. In this case, the extent of the site coverage is expected to be lower compared with the opposite case (winds from the south) when plumes from most areas of the site are very likely to cross a laser beam measurement path, and all areas in the gray boxes shown in Figure 1 would be covered. A relationship may therefore exist between the percent of site coverage and the emission rate wherein spuriously low emissions are estimated under a lower observational coverage.

To ensure that variability in the emission rate we estimate is due to changing emission rates and not the changing site coverage, we perform an initial processing step to remove low-coverage time periods from our analysis (Supporting Information Section 4). We find that samples with <30% site coverage are likely affected by a low bias because of insufficient site coverage but that samples with >30% site coverage are likely not. To be sure that 30% is not too low a threshold for site coverage, we additionally test a range of cutoff values (Supporting Information Section 4) and report emission rates calculated for a nominally higher value of >70% site coverage.

2.3. Aircraft-Based Mass Balance Measurements. Aircraft mass balance flights occurred at regular intervals during the measurement campaign. The mass balance flights use a stacked, closed-loop methodology whereby a virtual cylinder is traced by the airplane around the potential source area. The flux normal to the cylinder is calculated using instantaneous winds[35] and observed in situ methane concentrations. The path integral is then calculated for each loop to yield the average flux divergence of methane gas at the altitude of each loop according to Gauss' Theorem.[30] Most flights in this study involved 15−25 loops flown from ~70 m above ground level to a height above which no methane plumes were detected. Finally, the vertical integral of the flux divergences is calculated to yield a total emission rate for the area within the circle.
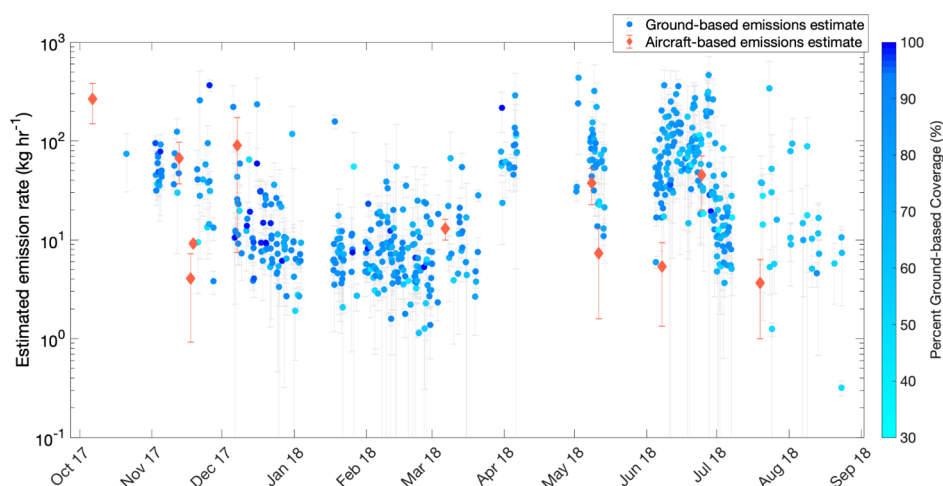
Figure 2. 3-hourly emission estimates (blue dots) of the ground-based DCS observing system and aircraft-based mass balance emission estimate (red diamonds) on a log scale. Gradation of color for the ground-based DCS observing system emission estimates represents the percent of equipment on site covered by observations in each 3 h period (color bar). Uncertainty bars are 1σ.
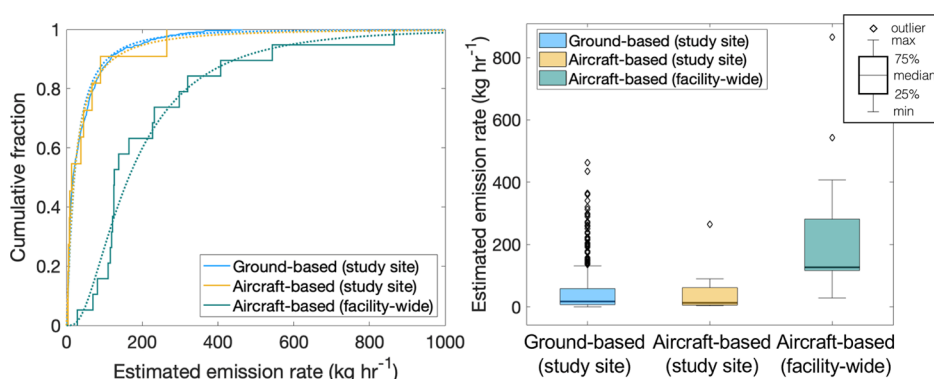

Figure 3. Empirical (solid step lines) and fitted (dotted curves) cumulative distribution functions (left panel) for the ground-based rates for the study site (blue), aircraft-based rates for the study site (yellow), and aircraft-based rates for the entire facility (teal). Box and whisker plots showing range, variability, and outliers for the estimated emission rates (right panel) for ground-based rates for the study site (blue, left box), aircraft-based rates for the study site (yellow, middle box), and aircraft-based rates for the entire facility (teal, right box).

An update to previous methods[30,35] is developed here, in which the slope in the lowest available 100 m altitude bin is extrapolated to the ground rather than assuming a constant value. The standard deviation of an individual loop flux within each 100 m bin is multiplied by the bin thickness (100 m) to obtain an error estimate for that bin. An error term for the total flux emission is then calculated by combining each bin's error term in a standard error propagation.[36]

During the measurement period of October 2017 through August 2018, 11 aircraft mass balance flights were performed. The average duration of airborne sampling measurements was 23 min.

3. RESULTS AND DISCUSSION

3.1. Atmospheric Concentration Measurements.
Atmospheric concentration measurements are made along open beam paths as shown in the site layout in Figure 1. The line-integrated concentrations are divided by the path length of the laser to yield path-averaged concentrations. Concentration measurements span a large range, from values near the global mean (the marine boundary layer global annual mean CH_4 dry-air mole fractions were 1849.65 ppb in 2017 and 1857.30 ppb in 2018[37]) to isolated peaks of up to ~42,000 ppb. The mean and standard deviation of all concentration measure-

ments is 3281 ± 2413 ppb and the median value is 2449 ppb. Several data gaps, evident in Figure 1, are due to two factors. First, this deployment was the first sustained, remote, autonomous field deployment of the DCS observing system. As such, multiple system upgrades were implemented during the 11-month field deployment, associated with lessons learned on the ground, including improved electrical power conditioning, better climate control of the laser system, and deterrents for wasps and birds in the telescope. Second, major on-site operations resulted in temporary blocking of some retroreflectors, a factor that has led to alternate beam path configurations in subsequent industrial deployments.

3.2. Study Site Emission Estimates.
We examine 3-hourly mean emissions (i.e., the average emission rate over 3 h in kg h^{-1}) at the study site (all areas shown in Figure 1) and aircraft-based estimates of emissions from the study site as well as from the entire facility. The time series of estimated emissions at the study site based on the DCS observing system and aircraft mass balance flights is shown in Figure 2. Substantial temporal variability and spread are evident in both the aircraft and DCS observing system estimates. The DCS observing system emission estimates shown in Figure 2 are shaded according to percent site coverage (Section 2.2).
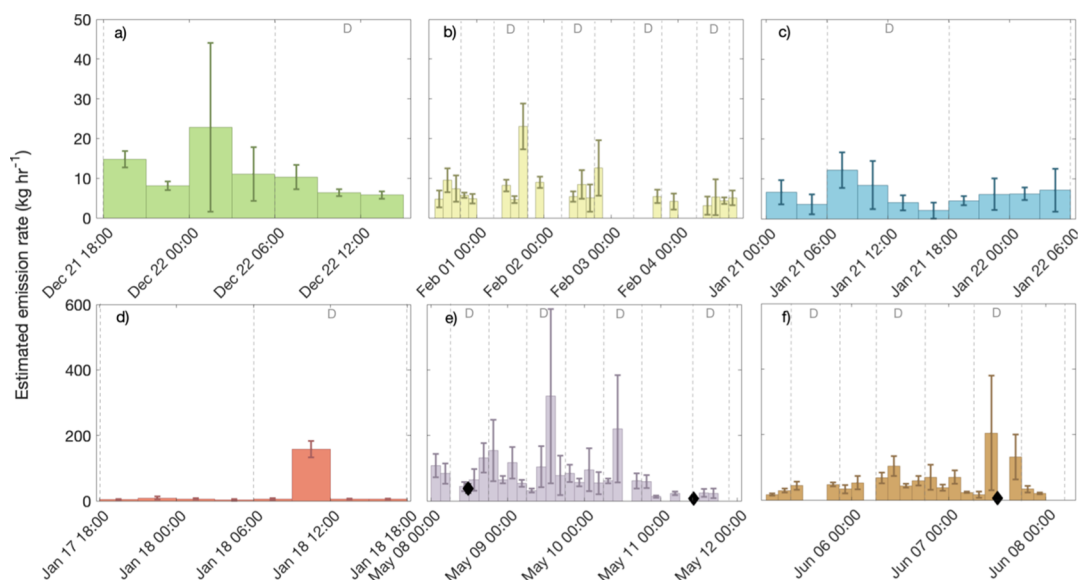
Figure 4. Ground-based DCS observing system emission estimates (bars) and aircraft-based mass balance emission estimates (black diamonds) for six time periods. (a−c) Time periods during which the variability in 3 h estimated emission rates is low compared with time periods shown in (d−f). Note the change in the *y*-axis from (a−c) to (d−f). Uncertainty bars are 1σ, and the width of each bar is 3 h. Dashed vertical gray lines distinguish day (6:00−18:00, labeled "D") from night.

3.3. Long-Term Emission Rates and Variability. The study site emission rates estimated by both the ground- and aircraft-based approaches are highly skewed. Figure 3 shows cumulative distributions of the emission rates. For the 3 h-average ground-based data, the maximum emission rate observed is 2.4 times the 95% fractile of the distribution. Finding that emission rates follow a lognormal distribution, we report the geometric mean for all emission time series. The emissions during all time periods (October 2017 through August 2018) are lognormally distributed (the mean and standard deviation of the log of the distribution are $\mu = 3.0$ and $\sigma = 1.3$) with a geometric mean rate of 20 [−2, +3] kg h^{-1} ($n = 560$) [95% confidence interval (CI)]. (For all lognormally distributed results, we report the geometric mean and 95% CI of the distribution.) Using a >70% site coverage threshold, the geometric mean emission rate is the same (20 [−3, +3] kg h^{-1}) and the lognormal distribution parameters are $\mu = 3.0$ and $\sigma = 1.5$.

During the same time period, the aircraft-based emission rates also follow a lognormal distribution with parameters of the log of the distribution of the data of $\mu = 3.0$ and $\sigma = 1.4$. The geometric mean of the aircraft-based estimated emission rates is 19.9 [−12.3, +32.0] kg h^{-1} ($n = 11$) (95% CI), indicating close agreement between the ground- and aircraft-based approaches.

The presence of more high outliers and a higher upper adjacent value in the continuous ground-based data, compared with the aircraft-based data, while the median and 25th and 75th percentile ranges and distributions are very similar, suggests that the increase in data density afforded by continuous monitoring allows for a fuller representation of the emission distribution (Figure 3). Indeed, the aircraft data only capture one outlier event, without which the distribution changes substantially with a geometric mean emission rate of only 15.3 [−8.8, +20.9] kg h^{-1}. We find that these outlier time periods comprise a critical proportion of overall emissions. The 10% highest 3 h emission periods observed by the continuous DCS observing system (outliers in Figure 3) comprise 41% of

the total observed 3-hourly emissions. This suggests that intermittent monitoring is very unlikely to accurately capture total emissions, compared with continuous monitoring.

Additional aircraft flights occurred before and after the DCS observing system campaign. The geometric mean of the estimated emission rates from all aircraft mass balance flights that occurred between October 2017 and June 2019 is 26.5 [−13.1, +26.0] kg h^{-1} ($n = 17$) (95% CI), with a lognormal distribution with log transform parameters $\mu = 3.3$ and $\sigma = 1.3$. Two-sample Kolmogorov−Smirnov testing of all three combinations of data (long-term and short-term aircraft, long-term aircraft and ground, and short-term aircraft and ground) confirms that they are from the same distribution. The agreement in distributions suggests that the time period of observation was sufficient to accurately capture the true distribution of emissions from the study area.

The emission rates demonstrate substantial variability through time, not only on shorter (day-to-day) but also on longer (month-to-month) time scales. Monthly geometric mean emission rates from the DCS observing system vary from a minimum of 6 [−2, +2] kg h^{-1} in February 2018 to a maximum of 85 [−22, +30] kg h^{-1} in April 2018 (Supporting Information Section 5). The aircraft-based emission estimates show an even wider range, although with a low number of monthly samples.

To better understand day-to-day and subdaily variability, we focus on several multiday periods in which favorable winds allowed for continuous observation of emissions from >30% of the site area. We examine three relatively low-variability time periods and three relatively high-variability time periods, including one time period during which a transient but large spike in emissions occurs. Figure 4a−c shows periods of relatively low variability in emissions and low mean emission rates overall. The geometric mean and full range of observed emission rates are 10 (6−23) , 6 (3−23), and 6 (2−12) kg h^{-1} for a−c, respectively. Figure 4d−f shows relatively higher and more variable emission rates. The geometric mean and range of observed emission rates are 9 (4−158), 66 (14−320), and
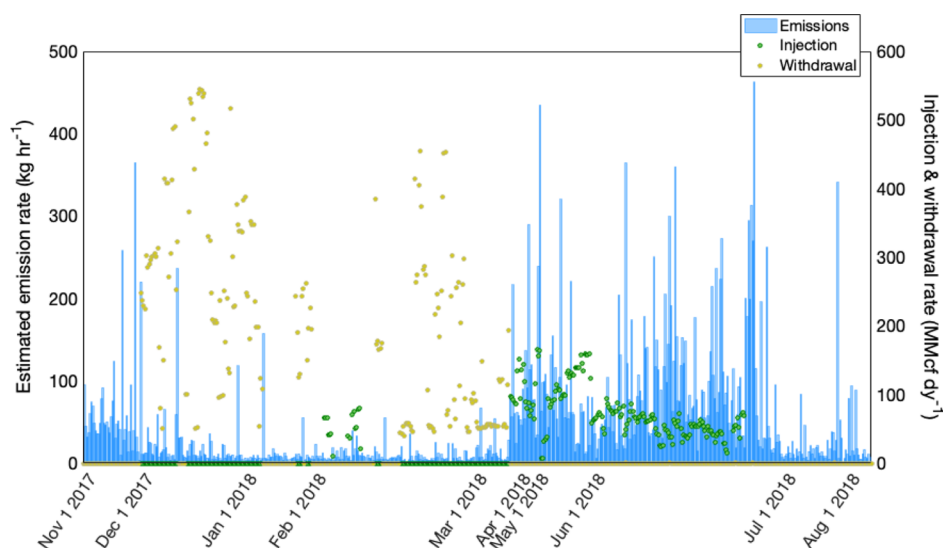
Figure 5. Time series of emissions (blue bars with a width of 3 h) with injection (green dot) and withdrawal (yellow dot) rates. Gaps in time series have been removed; the first day of each month is labeled on the x-axis.

46 (17−204) kg h^{-1} for d−f, respectively. The majority of the time period in Figure 4d shows emission rates below 10 kg h^{-1}; however, one 3 h period demonstrates a much higher emission rate of 158 ± 25 kg h^{-1} (1σ).

We examine the concentration data that are used to estimate the emission profiles in Figure 4d,e. One transient increase in emissions (Figure 4d) is associated with a spike in concentration measurements of roughly 30 ppm that is only 45 min in duration (Supporting Information Figure S3), indicating that even 3 h is too long a time period to fully capture the temporal variability in emissions at the site. The mean emission rate during the 3 h in which this event occurs is more than 17× the 24 h mean emission rate.

The high emission rate variability in Figure 4e is also accompanied by highly variable concentration measurements. Throughout the days of May 8−10, emission rates and atmospheric concentrations are both relatively high and variable, with a mean of 3.36 ppm and a range of 1.18−44.47 ppm (Supporting Information Figure S3). Beginning May 11, however, emission rates and atmospheric concentrations both return to lower values that vary less through time. Aircraft measurements made during the same 4-day period show a consistent signature of higher emissions during May 8−10 and lower emissions on May 11. Clustered aircraft flights during different time periods show similar variability; for example, three aircraft flights within a span of 7 days in November 2017 exhibit a nearly 17-fold difference (Figure 2). These examples highlight the uncertainties inherent in "snapshot" sampling of highly variable emission sources, as seen here, and underscore the importance of continuous monitoring for an accurate understanding of total emissions and for rapid identification of emission events in case they are driven, for example, by malfunctioning equipment that would benefit from rapid repair. Conversely, snapshots in time can capture large emissions that are not persistent and therefore overestimate total emissions through time. A snapshot, drive-by or fly-by emission estimate on the afternoon of May 10, for example, would have recorded an emission rate at least 8× higher than an estimation made the following day.

3.4. Comparison of the DCS Observing System and Aircraft Mass Balance. Periods of overlap between the

aircraft and DCS observing system sampling offer an opportunity to examine potential differences between the two methods. We reanalyze the DCS observing system data by examining emissions in 3 h windows centered on the time that each aircraft mass balance flight took place. In one instance, individual ensemble members have fewer than three downwind data points, so a 6 h window is used.

All concurrent aircraft and DCS observing system estimates agree to within 2σ uncertainty; however, some uncertainties are large for both methods, masking discrepancies. The overall root mean squared error between the estimated emission rates is 42 kg h^{-1}. A Bland−Altman analysis highlights differences between the methods based on the mean of both methods as a best estimate of the "true" value. No consistent bias is observed between methods, and all values fall within the 95% level of agreement (Supporting Information Section 9).

A recent study shows similar or greater magnitudes of discrepancy on same-day, same-facility flights using different aircraft emission estimation methods.[26] A possible source of the mismatch observed in our analysis is a difficulty in obtaining truly temporally concurrent estimates. Aircraft mass balance flights last only 23 min on average, compared with ground-based observation windows of several hours. Given the very short-term variability in the emission rates we observe (e.g., Figure 4), it may be expected that emission rates vary on shorter timescales than 3 h. While discrepancies are evident between some concurrent aircraft and DCS observing system estimates, the distributions of the long-term datasets are nonetheless very similar for the two methods (Figure 3). A future study using large eddy simulations of these data will yield further insights into potential drivers of the observed offsets of individual flight days.

3.5. Facility-Wide Emissions. In addition to aircraft mass balance flights that isolated emissions from the primary study site, a series of 19 flights characterizing the entire underground natural gas storage facility were performed between October 2017 and June 2019 (see Supporting Information Sections 1 and 7 and Figure S2 for details of the full facility and time series of emissions). Very high variability and skewness in emissions are recorded by the facility-wide mass balance flights (Figure 3). The geometric mean emission rate for the entire

time period is 164.6 [−51.8, +75.5] kg h^{-1} (95% CI), and the mean and standard deviation of the distribution of the log of emissions are μ = 5.1 and σ = 0.8. Despite the non-normal distribution of emissions, we examine the arithmetic mean facility-wide emission rate for comparison with past studies.[25] The arithmetic mean of the facility-wide emission rate is 222.1 ± 24.2 kg h^{-1} (2σ uncertainty) or roughly 4× the rate observed at the smaller section of the site. Two outliers drive the mean value higher (Figure 3 and Supporting Information Figure S2); removal of these outliers yields a mean rate of 165.3 kg h^{-1}. Both the arithmetic mean and the arithmetic mean with outliers removed are within the range of reported emission rates observed at other storage sites.[25,26] The drastic difference in the mean emission rate when outliers are and are not considered underscores the importance of either continuous or high-frequency, repeat measurement of storage facilities to allow for accurate capture of the true distribution of emission rates.

3.6. Comparison with Operations Data. To better understand potential sources of variability in the methane emission rate from the study site, we examine time series of operations data, including injection and withdrawal rates and leak detection and repair schedules. We find a statistically significant difference in emission rates during periods of injection (geometric mean rate of 56 [−7, +9] kg h^{-1}) compared with periods of withdrawal (8 [−1, +1] kg h^{-1}) (Figure 5 and Supporting Information Section 6). Similarly, CH$_4$ emissions as a percentage of the total gas flow rate (injection or withdrawal) are consistently higher during the injection phase compared with the withdrawal phase (Supporting Information Figure S1).

A statistically significant difference between emission rates estimated by the aircraft mass balance is not found; however, this is likely due to the significantly lower number of samples in the study period. For example, only two flights occurred during periods of withdrawal. While injection and withdrawal rates appear to be correlated with emission rates, relatively high emissions also occur at the beginning and end of the time series: periods during which neither injection nor withdrawal is occurring at the study site.

Higher emissions might be expected from some equipment, such as compressors, during injection and withdrawal because of the known methane slip associated with compression.[38] However, with no compressors on the study site (and the presence of gas conditioning equipment, which is used during withdrawal), it will remain the subject of future continuous monitoring studies with a higher spatial attribution to determine the source of higher emissions during injection. Analysis confirms that interference from compressor emissions did not skew our findings (Supporting Information Section 2). We therefore posit that the higher system pressures present during the injection phase could be driving pressure-based emission behavior.

Available work logs detailing locations and dates of leak detections and repair activities offer an opportunity for comparison with emissions. We find that a series of operations notes logged on 1/18/2018 coincide with the anomalous emission event shown in Figure 4d. The notes suggest the detection and logging of an issue with a series of well heads that the operator found to be below internal standards. We further find that the cessation of a nearly 3-day-long period of withdrawal at this section of the site coincides with the timing of the event shown in Figure 4 d. The site operator suggests

the possibility of maintenance or blowdown activity, although a detailed record of maintenance corresponding with the emission event is not available. We find that a series of notes on recommended repairs also coincide with other periods of transient, higher-emission rates from this section of the site. The finding that higher emissions are associated with repairs is confirmed by the site operator who reports that, typically, maintenance on well heads requires blowdown of the well head and the associated piping.

Finally, we find some evidence that daytime emissions differ from nighttime emissions depending upon the operating phase, but results are uncertain and require further investigation with additional data before conclusions can be drawn (Supporting Information Section 11).

3.7. Greenhouse Gas Inventory Relevant Numbers. This study produces, for the first time, long-term observations of variability in emissions from an underground natural gas storage facility. Nearly a full year of regular measurements allow for estimation of the full range of variability at the site measured. We find that a minimum of roughly monthly aircraft flights is necessary to adequately capture the distribution of emissions observed with continuous monitoring. If, for example, the aircraft flights had commenced just weeks later, missing the only outlier event captured by the aircraft, the distribution would have changed significantly (mean and standard deviation of the log of μ = 2.7 and σ = 1.2 compared with the aircraft−ground agreed on values of μ = 3.1 and σ = 1.3). This finding further underscores the importance of continuous or quasicontinuous (high frequency) monitoring for accurate capture of emission distributions from natural gas systems, including underground natural gas storage infrastructure.

We further compare available emission inventory numbers for the facility with our emission data. There is no inventory number for the smaller subsection of the site studied, only for the entire site. However, the 19 aircraft mass balance measurements of the entire underground natural gas storage facility (Section 3.5) are directly comparable to the facility-wide inventory estimate. We find good agreement between the inventory value of 1997 metric tons yr^{-1} and the aircraft-based estimated facility-wide mean and standard deviation of 1937 ± 1765 metric tons yr^{-1}. We report arithmetic mean and standard deviation for direct comparison with inventories and past studies.[25]

3.8. Implications and Opportunities for Future Mitigation Efforts. The findings of this work suggest that emissions from underground natural gas storage can vary substantially through time, with monthly geometric mean emission rates differing by more than 12× and 3-hourly mean emission rates varying by more than 17× in a 24 h period. We find a significant difference between emission rates during different operating phases of the facility (injection or withdrawal) and some evidence of higher emissions during logged work at the facility. These findings highlight the need for high-frequency or continuous monitoring for accurate emission quantification and characterization of emission distributions at underground natural gas storage facilities, as has been found for other sectors of the natural gas supply chain. In particular, this study supports the importance of Colorado's SB 19-181 legislation requiring that oil and gas operators (including in the storage segment) install continuous methane emissions monitors at facilities with large emissions potential.[16] The inclusion of quantified indicators of variability

in inventories will help end-users and stakeholders to appropriately contextualize temporally limited versus temporally continuous measurement campaigns. Finally, these findings offer insights into potential areas of focus for future emission mitigation activities.

■ ASSOCIATED CONTENT

ⓈⒾ Supporting Information

The Supporting Information is available free of charge at https://pubs.acs.org/doi/10.1021/acs.est.0c03175.

Details of storage site equipment, testing of potential interference from compressors, emission rates as a percentage of injection and withdrawal rates, facility-wide emission time series, overlapping aircraft and ground data time series, wellhead emissions, and analysis of diurnal variation in emissions (PDF)

■ AUTHOR INFORMATION

Corresponding Author

Caroline B. Alden − *Precision Laser Diagnostics Laboratory and Cooperative Institute for Research in Environmental Sciences, University of Colorado Boulder, Boulder, Colorado 80309, United States;* ⓞ orcid.org/0000-0002-5249-7800; Email: caroline.alden@colorado.edu

Authors

Robbie J. Wright − *Precision Laser Diagnostics Laboratory, University of Colorado Boulder, Boulder, Colorado 80309, United States*

Sean C. Coburn − *Precision Laser Diagnostics Laboratory, University of Colorado Boulder, Boulder, Colorado 80309, United States*

Dani Caputi − *University of California, Davis, California 95616, United States*

Griffith Wendland − *Precision Laser Diagnostics Laboratory, University of Colorado Boulder, Boulder, Colorado 80309, United States*

Alex Rybchuk − *Precision Laser Diagnostics Laboratory, University of Colorado Boulder, Boulder, Colorado 80309, United States*

Stephen Conley − *Scientific Aviation, Boulder, Colorado 80301, United States;* ⓞ orcid.org/0000-0001-6753-8962

Ian Faloona − *University of California, Davis, California 95616, United States*

Gregory B. Rieker − *Precision Laser Diagnostics Laboratory, University of Colorado Boulder, Boulder, Colorado 80309, United States*

Complete contact information is available at:
https://pubs.acs.org/10.1021/acs.est.0c03175

Author Contributions

The manuscript was written through contributions of all authors. All authors have given approval to the final version of the manuscript.

Notes

The authors declare the following competing financial interest(s): C. Alden, R. Wright, S. Coburn and G. Rieker disclose financial interest in the company LongPath Technologies Inc., a commercial entity that employs similar trace gas sensing and inversion techniques to those used in this study.

■ ACKNOWLEDGMENTS

■ REFERENCES

(1) Inventory of U.S. *Greenhouse Gas Emissions and Sinks 1990−2017*; EPA 430-R-19-001, 2019.

(2) Hayhoe, K.; Kheshgi, H. S.; Jain, A. K.; Wuebbles, D. J. Substitution of Natural Gas for Coal: Climatic Effects of Utility Sector Emissions. *Clim. Change* **2002**, *54*, 107−139.

(3) Alvarez, R. A.; Pacala, S. W.; Winebrake, J. J.; Chameides, W. L.; Hamburg, S. P. Greater Focus Needed on Methane Leakage from Natural Gas Infrastructure. *Proc. Natl. Acad. Sci.* **2012**, *109*, 6435−6440.

(4) Gilman, J. B.; Lerner, B. M.; Kuster, W. C.; de Gouw, J. A. Source Signature of Volatile Organic Compounds from Oil and Natural Gas Operations in Northeastern Colorado. *Environ. Sci. Technol.* **2013**, *47*, 1297−1305.

(5) Thompson, C. R.; Hueber, J.; Helmig, D. Influence of Oil and Gas Emissions on Ambient Atmospheric Non-Methane Hydrocarbons in Residential Areas of Northeastern Colorado. *Elem. Sci. Anth.* **2014**, *2*, 000035.

(6) Saunois, M.; Jackson, R. B.; Bousquet, P.; Poulter, B.; Canadell, J. G. The Growing Role of Methane in Anthropogenic Climate Change. *Environ. Res. Lett.* **2016**, *11*, 120207.

(7) Alvarez, R. A.; Zavala-Araiza, D.; Lyon, D. R.; Allen, D. T.; Barkley, Z. R.; Brandt, A. R.; Davis, K. J.; Herndon, S. C.; Jacob, D. J.; Karion, A.; Kort, E. A.; Lamb, B. K.; Lauvaux, T.; Maasakkers, J. D.; Marchese, A. J.; Omara, M.; Pacala, S. W.; Peischl, J.; Robinson, A. L.; Shepson, P. B.; Sweeney, C.; Townsend-Small, A.; Wofsy, S. C.; Hamburg, S. P. Assessment of Methane Emissions from the U.S. Oil and Gas Supply Chain. *Science* **2018**, *361*, No. eaar7204.

(8) Plant, G.; Kort, E. A.; Floerchinger, C.; Gvakharia, A.; Vimont, I.; Sweeney, C. Large Fugitive Methane Emissions From Urban Centers Along the U.S. East Coast. *Geophys. Res. Lett.* **2019**, *46*, 8500−8507.

(9) Brandt, A. R.; Heath, G. A.; Cooley, D. Methane Leaks from Natural Gas Systems Follow Extreme Distributions. *Environ. Sci. Technol.* **2016**, *50*, 12512−12520.

(10) Frankenberg, C.; Thorpe, A. K.; Thompson, D. R.; Hulley, G.; Kort, E. A.; Vance, N.; Borchardt, J.; Krings, T.; Gerilowski, K.; Sweeney, C.; Conley, S.; Bue, B. D.; Aubrey, A. D.; Hook, S.; Green, R. O. Airborne Methane Remote Measurements Reveal Heavy-Tail Flux Distribution in Four Corners Region. *Proc. Natl. Acad. Sci.* **2016**, *113*, 9734−9739.

(11) Zavala-Araiza, D.; Alvarez, R. A.; Lyon, D. R.; Allen, D. T.; Marchese, A. J.; Zimmerle, D. J.; Hamburg, S. P. Super-Emitters in Natural Gas Infrastructure Are Caused by Abnormal Process Conditions. *Nat. Commun.* **2017**, *8*, ncomms14012.

(12) Vaughn, T. L.; Bell, C. S.; Pickering, C. K.; Schwietzke, S.; Heath, G. A.; Pétron, G.; Zimmerle, D. J.; Schnell, R. C.; Nummedal, D. Temporal Variability Largely Explains Top-down/Bottom-up Difference in Methane Emission Estimates from a Natural Gas Production Region. *Proc. Natl. Acad. Sci.* **2018**, *115*, 11712−11717.

(13) Johnson, D.; Heltzel, R.; Oliver, D. Temporal Variations in Methane Emissions from an Unconventional Well Site. *ACS Omega* **2019**, *4*, 3708−3715.

(14) Heath, G. A. *Taxonomy, Life Cycle Assessment, and Meta-Analyses for Improving Methane Emissions Estimates from Oil and Gas*; NREL/PR-6A20-68478; National Renewable Energy Lab. (NREL): Golden, CO (United States), 2019.

(15) National Academies of Sciences Engineering, and Medicine. *Improving Characterization of Anthropogenic Methane Emissions in the United States*; National Academies Press: Washington, D.C., 2018.

(16) Protect Public Welfare Oil and Gas Operations Colorado General Assembly. https://leg.colorado.gov/bills/sb19-181 (accessed Jan 15, 2020).

(17) Lavoie, T. N.; Shepson, P. B.; Cambaliza, M. O. L.; Stirm, B. H.; Conley, S.; Mehrotra, S.; Faloona, I. C.; Lyon, D. Spatiotemporal Variability of Methane Emissions at Oil and Natural Gas Operations in the Eagle Ford Basin. *Environ. Sci. Technol.* **2017**, *51*, 8001−8009.

(18) U.S. Energy Information Administration (EIA) https://www.eia.gov/naturalgas/ngqs/#?report=RP7&year1=2018&year2=2018&company=Name (accessed Dec 2, 2019).

(19) Conley, S.; Franco, G.; Faloona, I.; Blake, D. R.; Peischl, J.; Ryerson, T. B. Methane Emissions from the 2015 Aliso Canyon Blowout in Los Angeles, CA. *Science* **2016**, *351*, 1317−1320.

(20) Michanowicz, D. R.; Buonocore, J. J.; Rowland, S. T.; Konschnik, K. E.; Goho, S. A.; Bernstein, A. S. A National Assessment of Underground Natural Gas Storage: Identifying Wells with Designs Likely Vulnerable to a Single-Point-of-Failure. *Environ. Res. Lett.* **2017**, *12*, 064004.

(21) Katz, D. L.; Tek, M. R. Overview on Underground Storage of Natural Gas. *J. Pet. Technol.* **1981**, *33*, 943.

(22) Schultz, R. A.; Hubbard, D. W.; Evans, D. J.; Savage, S. L. Characterization of Historical Methane Occurrence Frequencies from U.S. Underground Natural Gas Storage Facilities with Implications for Risk Management, Operations, and Regulatory Policy. *Risk Anal.* **2020**, *40*, 588.

(23) Subramanian, R.; Williams, L. L.; Vaughn, T. L.; Zimmerle, D.; Roscioli, J. R.; Herndon, S. C.; Yacovitch, T. I.; Floerchinger, C.; Tkacik, D. S.; Mitchell, A. L.; Sullivan, M. R.; Dallmann, T. R.; Robinson, A. L. Methane Emissions from Natural Gas Compressor Stations in the Transmission and Storage Sector: Measurements and Comparisons with the EPA Greenhouse Gas Reporting Program Protocol. *Environ. Sci. Technol.* **2015**, *49*, 3252−3261.

(24) Zimmerle, D. J.; Williams, L. L.; Vaughn, T. L.; Quinn, C.; Subramanian, R.; Duggan, G. P.; Willson, B.; Opsomer, J. D.; Marchese, A. J.; Martinez, D. M.; Robinson, A. L. Methane Emissions from the Natural Gas Transmission and Storage System in the United States. *Environ. Sci. Technol.* **2015**, *49*, 9374−9383.

(25) Mehrotra, S.; Faloona, I.; Suard, M.; Conley, S.; Fischer, M. L. Airborne Methane Emission Measurements for Selected Oil and Gas Facilities Across California. *Environ. Sci. Technol.* **2017**, *51*, 12981−12987.

(26) Thorpe, A. K.; et al. Methane Emissions from Underground Gas Storage in California. *Environ. Res. Lett.* **2020**, *15*, 045004.

(27) Coburn, S.; Alden, C. B.; Wright, R.; Cossel, K.; Baumann, E.; Truong, G.-W.; Giorgetta, F.; Sweeney, C.; Newbury, N. R.; Prasad, K.; Coddington, I.; Rieker, G. B. Regional Trace-Gas Source Attribution Using a Field-Deployed Dual Frequency Comb Spectrometer. *Optica* **2018**, *5*, 320.

(28) Alden, C. B.; Ghosh, S.; Coburn, S.; Sweeney, C.; Karion, A.; Wright, R.; Coddington, I.; Rieker, G. B.; Prasad, K. Bootstrap Inversion Technique for Atmospheric Trace Gas Source Detection and Quantification Using Long Open-Path Laser Measurements. *Atmos. Meas. Tech.* **2018**, *11*, 1565−1582.

(29) Alden, C. B.; Coburn, S. C.; Wright, R. J.; Baumann, E.; Cossel, K.; Perez, E.; Hoenig, E.; Prasad, K.; Coddington, I.; Rieker, G. B. Single-Blind Quantification of Natural Gas Leaks from 1 Km Distance Using Frequency Combs. *Environ. Sci. Technol.* **2019**, *53*, 2908−2917.

(30) Conley, S.; Faloona, I.; Mehrotra, S.; Suard, M.; Lenschow, D. H.; Sweeney, C.; Herndon, S.; Schwietzke, S.; Pétron, G.; Pifer, J.; Kort, E. A.; Schnell, R. Application of Gauss's Theorem to Quantify Localized Surface Emissions from Airborne Measurements of Wind and Trace Gases. *Atmos. Meas. Tech.* **2017**, *10*, 3345−3358.

(31) Coddington, I.; Newbury, N.; Swann, W. Dual-Comb Spectroscopy. *Optica* **2016**, *3*, 414−426.

(32) Waxman, E. M.; Cossel, K. C.; Truong, G.-W.; Giorgetta, F. R.; Swann, W. C.; Coburn, S.; Wright, R. J.; Rieker, G. B.; Coddington, I.; Newbury, N. R. Intercomparison of Open-Path Trace Gas Measurements with Two Dual Frequency Comb Spectrometers. *Atmos. Meas. Tech.* **2017**, *10*, 3295−3311.

(33) Coddington, I.; Newbury, N.; Swann, W. Dual-Comb Spectroscopy. *Optica* **2016**, *3*, 414−426.

(34) Coburn, S.; Alden, C. B.; Wright, R.; Wendland, G.; Rybchuk, A.; Seitz, N.; Coddington, I.; Rieker, G. B. Long Distance Continuous Methane Emissions Monitoring with Dual Frequency Comb Spectroscopy: Deployment and Blind Testing in Complex Emissions Scenarios. **2020**, arXiv:physics/2009.10853. https://arxiv.org/ftp/arxiv/papers/2009/2009.10853.pdf.

(35) Conley, S. A.; Faloona, I. C.; Lenschow, D. H.; Karion, A.; Sweeney, C. A Low-Cost System for Measuring Horizontal Winds from Single-Engine Aircraft. *J. Atmos. Ocean. Technol.* **2014**, *31*, 1312−1320.

(36) Caputi, S. D. Meteorological Conditions Surrounding California's Central Valley High Ozone Events: An Integrative Approach. Ph.D. Dissertation, University of California Davis, 2019.

(37) Dlugokencky, E. J. NOAA/ESRL. Www.Esrl.Noaa.Gov/Gmd/Ccgg/Trends_ch4/ (accessed February 1, 2020).

(38) Johnson, D. R.; Covington, A. N.; Clark, N. N. Methane Emissions from Leak and Loss Audits of Natural Gas Compressor Stations and Storage Facilities. *Environ. Sci. Technol.* **2015**, *49*, 8132−8138.